Engineering Fracture Mechanics 78 (2011) 175–190

Contents lists available at ScienceDirect

Engineering Fracture Mechanics

journal homepage: www.elsevier.com/locate/engfracmech

An enriched radial point interpolation method (e-RPIM) for analysis of crack tip fields

Y.T. Gu [a,*], W. Wang [a], L.C. Zhang [b], X.Q. Feng [c]

[a] School of Engineering Systems, Queensland University of Technology, GPO Box 2434, Brisbane QLD 4001, Australia
[b] School of Mechanical and Manufacturing Engineering, The University of New South Wales, Sydney NSW 2052, Australia
[c] AML, Department of Engineering Mechanics, Tsinghua University, Beijing 100084, China

ARTICLE INFO

Article history:
Received 27 January 2010
Received in revised form 8 June 2010
Accepted 27 October 2010
Available online 3 November 2010

Keywords:
Fracture mechanics
Meshfree method
Crack tip
RBF
Enriched RPIM

ABSTRACT

In this paper, an enriched radial point interpolation method (e-RPIM) is developed for the determination of crack tip fields. In e-RPIM, the conventional RBF interpolation is novelly augmented by the suitable trigonometric basis functions to reflect the properties of stresses for the crack tip fields. The performance of the enriched RBF meshfree shape functions is firstly investigated to fit different surfaces. The surface fitting results have proven that, comparing with the conventional RBF shape function, the enriched RBF shape function has: (1) a similar accuracy to fit a polynomial surface; (2) a much better accuracy to fit a trigonometric surface; and (3) a similar interpolation stability without increase of the condition number of the RBF interpolation matrix. Therefore, it has proven that the enriched RBF shape function will not only possess all advantages of the conventional RBF shape function, but also can accurately reflect the properties of stresses for the crack tip fields. The system of equations for the crack analysis is then derived based on the enriched RBF meshfree shape function and the meshfree weak-form. Several problems of linear fracture mechanics are simulated using this newly developed e-RPIM method. It has demonstrated that the present e-RPIM is very accurate and stable, and it has a good potential to develop a practical simulation tool for fracture mechanics problems.

1. Introduction

Understanding the deformation mechanisms and stress fields at crack tips is essential for the safety assessment and life prediction of engineering structures. Due to the stress singularity and nonlinear features of crack tip fields, their solutions are usually difficult to be obtained analytically. In recent times, the finite element method (FEM) is a dominant numerical tool in the analysis of fracture problems, especially for stationary cracks. However, FEM has some distinct shortcomings [1] particularly for dynamic cracks. To overcome these shortcomings, the concept of meshless or meshfree method has been proposed [2].

Recently, much effort has been directed towards the development of meshfree methods. Detailed reviews of meshfree methods can be found in, e.g., monographs [2,3]. There are many categories of meshfree methods [2], and a group of meshfree methods have been developed including the meshfree collocation methods [4], the smooth particle hydrodynamics (SPH) [5], the element-free Galerkin (EFG) method [6], the reproducing kernel particle method (RKPM) [7], and the point interpolation method (PIM) [8]. To alleviate the global integration background cells, the meshfree methods based on the local weak-forms and the boundary integral equation (BIE) have also been developed, including the meshless local

* Corresponding author.
E-mail address: yuantong.gu@qut.edu.au (Y.T. Gu).

0013-7944/$ - see front matter © 2010 Elsevier Ltd. All rights reserved.
doi:10.1016/j.engfracmech.2010.10.014

Nomenclature

$\mathbf{a}$, $\mathbf{b}$, $\mathbf{c}$	vector of interpolation coefficients, defined in Eq. (7)
$\mathbf{B}$	matrix for derivatives of shape function defined in Eq. (23)
$\mathbf{D}$	matrix of material constants, defined in Eq. (23)
e_t, e_c	computational error indicators, defined in Eqs. (32) and (33)
E	Young's modulus
$\mathbf{f}$	vector of body force, defined in Eq. (18)
$\mathbf{F}$	force vectors for the meshfree method, defined in Eq. (22)
f_1, f_2	functions to be fitted, defined in Eqs. (34) and (35)
$\mathbf{G}$	total interpolation matrix, defined in Eq. (12)
J	J integral for crack, defined in Eq. (24)
K_I, K_{II}, K_{III}	stress intensity factors for mode-I, mode-II , and mode-III
$\mathbf{K}$	stiffness matrix the meshfree method, defined in Eq. (22)
$\mathbf{n}$	vector of the unit outward normal, defined in Eq. (19)
$\mathbf{P}$,$\mathbf{R}$	vectors for polynomial and RBF basis functions defined in Eq. (7)
$\mathbf{T}$	vectors for enriched trigonometric basis functions defined in Eq. (6)
$\mathbf{P_m}$, $\mathbf{R_0}$, $\mathbf{T_l}$	interpolation matrixes for enriched RBF defined in Eq. (9)
R	radial basis function (RBF), defined in Table 1
(r,θ)	cylindrical coordinate, defined in Eqs. (1)–(4)
$\mathbf{u}$	displacement vector, defined in Eqs. (1), (3) and (20)
$\mathbf{u_e}$	nodal displacement vector used in interpolation, defined in Eq. (8)
$\bar{\mathbf{u}}$, $\bar{\mathbf{t}}$	prescribed boundary displacement and traction, defined in Eq. (19)
$\mathbf{x}$	coordinate vector
Γ	global boundary
κ	Kolosov constant
ν	Poisson's ratio
ϕ	shape function, defined in Eq. (16)
$\mathbf{\Phi}$	shape function vector, defined in Eq. (16)
Π	functional
Γ_u, Γ_t	boundaries for displacement and traction boundary conditions, defined in Eq. (19)
$\boldsymbol{\varepsilon}$, $\boldsymbol{\sigma}$	vectors of strain and stress, defined in Eqs. (2), (4), (19) and (20)
τ	shear stress
Ω	problem domain

Petrov-Galerkin (MLPG) method [9], the local radial point interpolation method (LRPIM) [10], the boundary node method (BNM) [11], and the boundary point interpolation method (BPIM) [12,13]. These meshfree methods have found many applications in engineering and science [3].

In spite of the impressive progresses, there are still some technical issues in the development of meshfree techniques, for instance, (a) the lack of theoretical study on the computational convergence and stability; (b) the relatively worse computational efficiency; and (c) the lack of commercial software packages for meshfree analyses. Recently, some deep researches have been conducted and the above issues have been partially resolved. Liu et al. [14,15] proposed a node-based smoothed point interpolation method (NS-PIM), which is formulated using the polynomial point interpolation method (PIM) [8] or the radial point interpolation method (RPIM) [16]. It was found that NS-PIM behaves 'overly-soft', leading to the so-called temporal instability when it is used to solve dynamic problems. The formulation was also elaborated with a theoretical base on the G space theory [1]. Invoking the G space theory and the weakened weak-form (W^2) [17], the meshfree (or smoothed FEM) methods show a number of attractive properties, e.g., conformability, softness, upper/lower bound, super-convergence, ultra accuracy, and they also work well with triangular background cells [1] . Another new development in meshless techniques is the developments of the class of smoothed meshfree methods, Smoothed Point Interpolation Method (S-PIM) and Smoothed FEM (S-FEM)[18]. These smoothed meshless methods have many advantages, including no mapping needed, excellent performance for triangular/tetrahedral cells, and insensitive to cell distortion. Because of the unique advantages, S-PIM and S-FEM have been successfully applied to fracture problems. [19,20].

As above discussed, meshfree methods do not require a mesh to discretize the problem domain, and the approximate solution is constructed entirely by a set of scattered nodes. The principal attraction of meshfree methods is their capacity in dealing with problems with moving boundaries and discontinuities, for instance, phase transition and crack propagation problems, and their ease in using the enriched basis functions based on the asymptotic displacement fields near the crack tip [21]. Among others, EFG, which is based on the moving least squares (MLS) and the enriched weight/basis functions, has been successfully applied to fracture problems [21–23].

The radial point interpolation method (RPIM) proposed by Liu and coworkers [2,16] takes use of the radial basis function (RBF) and have some attractive properties, including the robustness in interpolation, good performance for irregular nodes,

good accuracy, and delta properties for easy implementation of essential boundary conditions. Therefore, RPIM has been successfully used in the analysis of solids, fluids and composite materials [2,24]. Although many researches have proven that RPIM based on the conventional RBF augmented by polynomial has very good accuracy for problems with polynomial solutions, it cannot accurately reproduce the stress field of the crack tip due to its' nature of singularity and complex non-polynomial solutions, e.g., the trigonometric solutions. Therefore, there is little application of conventional RPIM for fracture problems.

In this paper, an enriched radial point interpolation method (e-RPIM) is developed for the determination of crack tip fields. The conventional RBF interpolation [2] is novelly augmented by the trigonometric basis functions to reflect the properties of the crack tip stress fields. The performance of the enriched RBF meshfree shape functions is firstly investigated through the surface fitting. Then, the system of equations for the 2-D crack analysis is derived based on the enriched RBF meshfree shape function and the meshfree weak-form. Several crack problems are simulated by this newly developed e-RPIM. A parametric comparison with the results in the literature and from analytical solutions shows that the present e-RPIM is accurate, efficient and effective for the analysis of crack tip fields.

2. enriched RBF shape functions

2.1. Enriched basis function

In two-dimensional (2-D) linear elastic fracture mechanics (LEFM), both mode-I and mode-II crack tip fields should be considered. The mode-I and mode-II crack tip fields are expressed as [25,26]

$$\text{Mode I}: \left\{ \begin{matrix} u_1 \\ u_2 \end{matrix} \right\} = \frac{K_I}{2\mu}\sqrt{\frac{r}{2\pi}} \left\{ \begin{matrix} \cos\left(\frac{\theta}{2}\right)\left[\kappa - 1 + 2\sin^2\left(\frac{\theta}{2}\right)\right] \\ \sin\left(\frac{\theta}{2}\right)\left[\kappa + 1 - 2\cos^2\left(\frac{\theta}{2}\right)\right] \end{matrix} \right\} \tag{1}$$

$$\left\{ \begin{matrix} \sigma_{11} \\ \sigma_{22} \\ \sigma_{12} \end{matrix} \right\} = \frac{K_I}{\sqrt{2\pi r}}\cos\frac{\theta}{2} \left\{ \begin{matrix} 1 - \sin\frac{\theta}{2}\sin\frac{3\theta}{2} \\ 1 + \sin\frac{\theta}{2}\sin\frac{3\theta}{2} \\ \sin\frac{\theta}{2}\sin\frac{3\theta}{2} \end{matrix} \right\} \tag{2}$$

$$\text{Mode II}: \left\{ \begin{matrix} u_1 \\ u_2 \end{matrix} \right\} = \frac{K_{II}}{2\mu}\sqrt{\frac{r}{2\pi}} \left\{ \begin{matrix} \sin\left(\frac{\theta}{2}\right)\left[\kappa + 1 + 2\cos^2\left(\frac{\theta}{2}\right)\right] \\ -\cos\left(\frac{\theta}{2}\right)\left[\kappa - 1 - 2\sin^2\left(\frac{\theta}{2}\right)\right] \end{matrix} \right\} \tag{3}$$

$$\left\{ \begin{matrix} \sigma_{11} \\ \sigma_{22} \\ \sigma_{12} \end{matrix} \right\} = \frac{K_{II}}{\sqrt{2\pi r}}\cos\frac{\theta}{2} \left\{ \begin{matrix} -\sin\frac{\theta}{2}\left(2 + \cos\frac{\theta}{2}\cos\frac{3\theta}{2}\right) \\ \sin\frac{\theta}{2}\cos\frac{\theta}{2}\cos\frac{3\theta}{2} \\ \cos\frac{\theta}{2}\left(1 - \sin\frac{\theta}{2}\sin\frac{3\theta}{2}\right) \end{matrix} \right\} \tag{4}$$

where K_I and K_{II} are the stress intensity factors (SIF) for mode-I and mode-II dependent upon the crack length, the specimen geometry and the applied loading, and (r,θ) are the cylindrical coordinates of a point with the origin located at the crack tip and the positive angle measured counterclockwise from the axis of the crack. κ is the Kolosov constant defined as,

$$\kappa = \begin{cases} 3 - 4\upsilon & \text{plane strain} \\ (3-\upsilon)/(1+\upsilon) & \text{plane stress} \end{cases} \tag{5}$$

After using trigonometric identities, one can show that all of the functions in Eqs. (1)–(4) are spanned by the following four basis functions [26]:

$$\mathbf{T} = \left\{ \sqrt{r}\cos\frac{\theta}{2} \quad \sqrt{r}\sin\frac{\theta}{2} \quad \sqrt{r}\sin\frac{\theta}{2}\sin\theta \quad \sqrt{r}\cos\frac{\theta}{2}\sin\theta \right\}^T \tag{6}$$

In the application of the meshfree method to linear elastic fracture mechanics (LEFM) problems, it is advantageous to add these four basis functions into the interpolation so that the stress singularity can be captured without having a very fine nodal density around the crack tip. It was first used by Fleming et al. [21] in the element-free Galerkin (EFG) method, based on the moving least squares approximation (MLSA), and called the resulting basis as enriched basis functions. It should be mentioned here that, comparing with FEM, the meshfree method provides possibility to include these enriched basis functions because of the freedom in construction of meshfree shape functions [2].

2.2. Construction of enriched RBF meshfree shape function

At present, a number of ways to construct meshfree shape functions have been proposed [2]. In this paper, the radial basis function (RBF) [2] interpolation augmented by the polynomial basis functions and the trigonometric basis functions given in

Eq. (6) is used to construct the meshfree shape functions. The locally supported enriched RBF interpolation formulation can be written as:

$$u(\mathbf{x}) = \sum_{i=1}^{n} R_i(r)a_i + \sum_{j=1}^{m} p_j(\mathbf{x})b_j + \sum_{l=1}^{4} t_l(\mathbf{x})c_l = \mathbf{R}^T\mathbf{a} + \mathbf{P}^T\mathbf{b} + \mathbf{T}^T\mathbf{c} = \left\{\mathbf{R}^T \quad \mathbf{P}^T \quad \mathbf{T}^T\right\}\begin{Bmatrix}\mathbf{a}\\ \mathbf{b}\\ \mathbf{c}\end{Bmatrix} \tag{7}$$

where $R_i(r)$ is the RBF, n is the number of nodes in the interpolation domain of point $\mathbf{x}$, $p_j(\mathbf{x})$ is monomials, m is the number of polynomial basis functions, $t_l(\mathbf{x})$ is the trigonometric basis function given in Eq. (6), and a_i, b_j and c_l are interpolation coefficients.

It should mention here that in Eq. (7), the trigonometric basis functions $\mathbf{T}$ are augmented in order to capture the singular stress field around the crack tip. In the conventional RBF interpolation, the RBF is only augmented by the polynomial basis function which is not always necessary. The objectives to add the polynomial base functions are summarized as:

(1) Adding polynomial terms up to the linear order can ensure the C^1 consistency for the RBF shape function, because the C^1 consistency is essential to exactly pass the standard patch test;
(2) in general, adding polynomial terms can always improve the accuracy of the results, at least no bad effect has been observed for meshfree weak-form methods;
(3) adding polynomial terms reduces the sensitivity of the shape parameters of RBF, and will provide us much more freedom and a wider range in choosing shape parameters; and
(4) adding polynomial terms can improve the interpolation stability for some RBFs [27,28].

There are a number of RBFs, such as the Multi-quadrics (MQ), Gaussian (EXP) and Thin Plate Spline (TPS). Their characters in meshfree methods have been carefully investigated by many researchers [27,29]. These three types of RBFs and their shape parameters used in this paper can be found in Table 1.

In order to determine interpolation coefficients in Eq. (7), an interpolation domain is formed for the point of interest at $\mathbf{x}$, and n field nodes are included in this interpolation domain. Coefficients in Eq. (7) can be determined by enforcing Eq. (7) to be satisfied at these n nodes to lead to n linear equations, one for each node. The matrix form of these equations can be expressed as

$$\mathbf{u}_e = \{u_1 \quad u_2 \quad \cdots \quad u_n\}^T = \mathbf{R}_0\mathbf{a} + \mathbf{P}_m\mathbf{b} + \mathbf{T}_l\mathbf{c} \tag{8}$$

where $\mathbf{R}_0$, $\mathbf{P}_m$ and $\mathbf{T}_l$ are matrixes for RBF, polynomial basis functions and trigonometric basis functions, respectively, i.e.

$$\mathbf{R}_0 = \begin{bmatrix} R_1(r_1) & R_2(r_1) & \cdots & R_n(r_1)\\ R_1(r_2) & R_2(r_2) & \cdots & R_n(r_2)\\ \vdots & \vdots & \ddots & \vdots\\ R_1(r_n) & R_2(r_n) & \cdots & R_n(r_n)\end{bmatrix}\Bigg|_{n\times n}, \tag{9}$$

$$\mathbf{P}_m^{\mathrm{T}} = \begin{bmatrix} p_1(\mathbf{x}_1) & p_1(\mathbf{x}_2) & \cdots & p_1(\mathbf{x}_n)\\ p_2(\mathbf{x}_1) & p_2(\mathbf{x}_2) & \cdots & p_2(\mathbf{x}_n)\\ \vdots & \vdots & \ddots & \vdots\\ p_m(\mathbf{x}_1) & p_m(\mathbf{x}_2) & \cdots & p_m(\mathbf{x}_n)\end{bmatrix}\Bigg|_{m\times n},$$

$$\mathbf{T}_l^{\mathrm{T}} = \begin{bmatrix} T_1(\mathbf{x}_1) & T_1(\mathbf{x}_2) & \cdots & T_1(\mathbf{x}_n)\\ T_2(\mathbf{x}_1) & T_2(\mathbf{x}_2) & \cdots & T_2(\mathbf{x}_n)\\ \vdots & \vdots & \ddots & \vdots\\ T_l(\mathbf{x}_1) & T_l(\mathbf{x}_2) & \cdots & T_l(\mathbf{x}_n)\end{bmatrix}\Bigg|_{l\times n}$$

Table 1
The employed parameters for RBFs.

Name	RBF	Shape parameter [2]
Multi-quadrics (MQ)	$R_i(\mathbf{x}) = \left[r_i^2 + (\alpha_c d_c)^2\right]^q$	$\alpha_c = 1.0$, $q = 1.03$ or $q = 0.98$
Gaussian (EXP)	$R_i(\mathbf{x}) = \exp\left[-\alpha_c\left(\frac{r_i}{d_c}\right)^2\right]$	$\alpha_c = 0.31$
Thin Plate Spline (TPS)	$R_i(\mathbf{x}) = r_i^\eta$	$\eta = 2.01$

However, in Eq. (8), there are only n equations for $n + m + l$ variables. To obtain unique solution, additional $m + l$ equations should be added, which are the $m + l$ constraint conditions, i.e.

$$\sum_{i=1}^{n} p_j(\mathbf{x}_i)a_i = \mathbf{P}_m^{\mathrm{T}}\mathbf{a} = 0, \quad j = 1, 2, \ldots, m \tag{10}$$

$$\sum_{i=1}^{n} T_j(\mathbf{x}_i)a_i = \mathbf{T}_l^{\mathrm{T}}\mathbf{a} = 0, \quad j = 1, 2, \ldots, l \tag{11}$$

Combining Eqs. (8), (10) and (11) yields the following set of equations in matrix format, i.e.

$$\left\{ \begin{array}{c} \mathbf{u_e} \\ \mathbf{0} \\ \mathbf{0} \end{array} \right\} = \left[\begin{array}{ccc} \mathbf{R}_0 & \mathbf{P}_m & \mathbf{T}_l \\ \mathbf{P}_m^{\mathrm{T}} & 0 & 0 \\ \mathbf{T}_l^{T} & 0 & 0 \end{array} \right]\Bigg|_{(n+m+l)\times(n+m+l)} \cdot \left\{ \begin{array}{c} \mathbf{a} \\ \mathbf{b} \\ \mathbf{c} \end{array} \right\}\Bigg|_{(n+m+l)\times 1} = \mathbf{G}\mathbf{a}_0 \tag{12}$$

where

$$\mathbf{a}_0 = \{a_1 \ \cdots \ a_n \ b_1 \ \cdots \ b_m \ c_1 \ \cdots \ c_l\}^T \tag{13}$$

From Eq. (12), the vector of interpolation coefficients $\mathbf{a}_0$ can be solved, i.e.,

$$\mathbf{a}_0 = \left\{ \begin{array}{c} \mathbf{a} \\ \mathbf{b} \\ \mathbf{c} \end{array} \right\}\Bigg|_{(n+m+l)\times 1} = \mathbf{G}^{-1} \left\{ \begin{array}{c} \mathbf{u_e} \\ \mathbf{0} \\ \mathbf{0} \end{array} \right\} \tag{14}$$

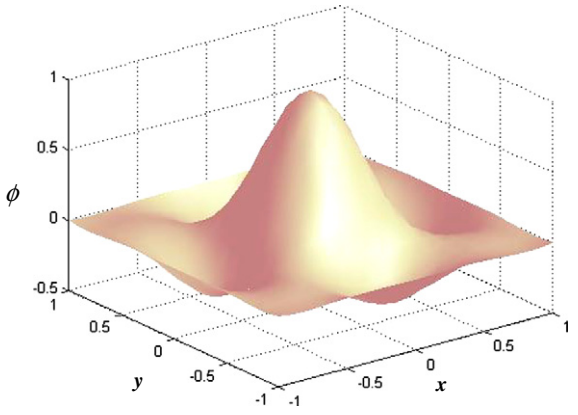

(a) Enriched RBF shape function

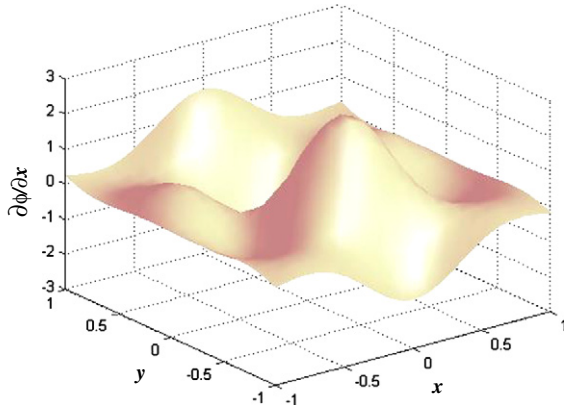

(b) The first order derivative of enriched RBF shape function

Fig. 1. The enriched MQ RBF meshfree shape functions and their derivatives.

Therefore, the following enriched RBF interpolation formulation is then obtained by substituting $\mathbf{a}_0$ into Eq. (7):

$$u(\mathbf{x}) = \left\{\mathbf{R}^T \quad \mathbf{P}^T \quad \mathbf{T}^T\right\}\mathbf{G}^{-1}\begin{Bmatrix}\mathbf{u}_e\\0\\0\end{Bmatrix} = \{\mathbf{\Phi}(\mathbf{x}) \quad \mathbf{\Lambda}(\mathbf{x}) \quad \mathbf{\Psi}(\mathbf{x})\}\begin{Bmatrix}\mathbf{u}_e\\0\\0\end{Bmatrix} = \mathbf{\Phi}(\mathbf{x})\mathbf{u}_e + \mathbf{\Lambda}(\mathbf{x})\cdot\mathbf{0} + \mathbf{\Psi}(\mathbf{x})\cdot\mathbf{0} = \mathbf{\Phi}(\mathbf{x})\mathbf{u}_e \tag{15}$$

where the enriched RBF meshfree shape functions can be expressed as

$$\mathbf{\Phi}(\mathbf{x}) = \{\phi_1(\mathbf{x}) \quad \phi_2(\mathbf{x}) \quad \cdots \quad \phi_n(\mathbf{x})\}^T = \left\{\mathbf{R}^T \quad \mathbf{P}^T \quad \mathbf{T}^T\right\}\mathbf{G}^{-1}\Big|_{1\sim n} \tag{16}$$

Fig. 1 shows the enriched MQ RBF meshfree shape functions and their derivatives. The shape parameters for MQ are used as $a_c = 2.0$, $d_c = 0.5$, and $q = 0.5$. From Fig. 1, we can clearly see that an enriched RBF shape functions have high continuity. As discussed by Liu and Gu [2,30], the RBF interpolation may not satisfy the partition of unity (the summation of shape functions is 1.0 [13]) exactly without polynomial augmented. However, if the constant term is included in the augmented polynomial basis functions, it has been found the enriched RBF shape functions can satisfy the partition of unity exactly.

In addition, the enriched RBF shape functions also have the Kronecker delta function property. For example, in Fig. 1a, at point $\mathbf{x}^{\mathrm{T}} = [0,0]$, where nodal number is 13, we have

$$\phi_i(x) = \begin{cases} 1 & i = 13 \ (\mathbf{x} = \mathbf{x}_{13}) \\ 0 & i \neq 13 \ (\mathbf{x} \neq \mathbf{x}_{13}) \end{cases} \tag{17}$$

This confirms numerically that the enriched RBF meshfree shape functions possess the Kronecker delta function property. It can be also proven theoretically [2]. The Kronecker delta condition allows a straightforward imposition of boundary conditions. Hence, it makes easy to enforce the essential boundary conditions in the meshfree method based on the enriched RBF shape functions. Comparing with other meshfree shape functions, the delta property is one of distinguished advantages of the enriched RBF meshfree shape function.

3. Enriched RPIM (E-RPIM)

3.1. Discrete equations of e-RPIM

Consider the following 2-D problem of solid mechanics in domain Ω bounded by Γ [2]:

$$\nabla\boldsymbol{\sigma} + \mathbf{f} = 0 \quad \text{in } \Omega \tag{18}$$

The boundary conditions are given as follows:

$$\mathbf{u} = \bar{\mathbf{u}} \quad \text{on } \Gamma_u; \qquad \sigma\cdot\mathbf{n} = \bar{\mathbf{t}} \qquad \text{on } \Gamma_t \tag{19}$$

The principle of minimum potential energy can be stated as follows: The solution of a problem in the small displacement theory of elasticity is the vector function $\mathbf{u}$ which minimizes the total potential energy Π given by

$$\Pi = \int_\Omega \frac{1}{2}\boldsymbol{\varepsilon}^{\mathrm{T}}\cdot\boldsymbol{\sigma}\,\mathrm{d}\Omega - \int_\Omega \mathbf{u}^{\mathrm{T}}\cdot\mathbf{f}\,\mathrm{d}\Omega - \int_{\Gamma_t}\mathbf{u}^{\mathrm{T}}\cdot\bar{\mathbf{t}}\,\mathrm{d}\Gamma \tag{20}$$

with the boundary conditions described in Eq. (19), where $\boldsymbol{\varepsilon}$ is the strain vector. Substituting the expression of $\mathbf{u}$ given in Eq. (15), and using the stationary condition for Eq. (20) yields the following discrete equation of e-RPIM:

$$\mathbf{KU} = \mathbf{F} \tag{21}$$

where $\mathbf{K}$, $\mathbf{U}$, and $\mathbf{F}$ are stiffness matrices, the displacement vectors, and the force vectors for e-RPIM, i.e.,

$$\begin{aligned}\mathbf{K}_{ij} &= \int_\Omega \mathbf{B}_i^{\mathrm{T}}\mathbf{D}\mathbf{B}_j\,\mathrm{d}\Omega \\ \mathbf{F}_i &= \int_{\Gamma_t}\phi_i\bar{\mathbf{t}}\mathrm{d}\Gamma + \int_\Omega \phi_i\mathbf{f}\,\mathrm{d}\Omega\end{aligned} \tag{22}$$

where $\mathbf{B}$ and $\mathbf{D}$ are

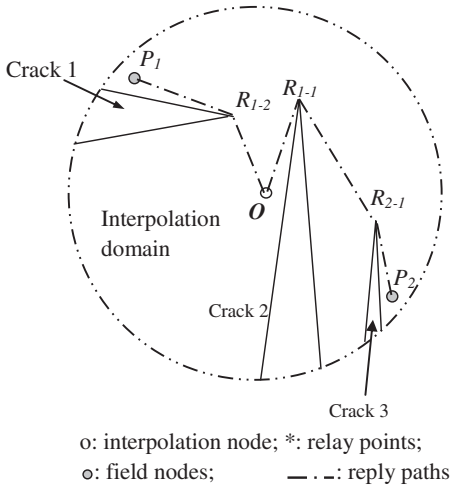

Fig. 2. The Relay model for multi-cracking problems [23].

$$\mathbf{B}_i = \begin{bmatrix} \phi_{i,x} & 0 \\ 0 & \phi_{i,y} \\ \phi_{i,y} & \phi_{i,x} \end{bmatrix},$$

$$\mathbf{D} = \frac{E}{(1+\upsilon)(1-2\upsilon)} \begin{bmatrix} 1-\upsilon & \upsilon & 0 \\ \upsilon & 1-\upsilon & 0 \\ 0 & 0 & \frac{1}{2}-\upsilon \end{bmatrix} \text{ plane strain} \tag{23}$$

$$\mathbf{D} = \frac{E}{(1-\upsilon^2)} \begin{bmatrix} 1 & \upsilon & 0 \\ \upsilon & 1 & 0 \\ 0 & 0 & \frac{1-\upsilon}{2} \end{bmatrix} \text{ plane stress}$$

3.2. The relay model

With the use of nodal based interpolation techniques, the meshfree methods offer great opportunities to handle problems with complex geometry including cracks. However, there is general discontinuity of displacements across a crack, and the interpolation domain used for the construction of meshfree shape functions can contain numerous irregular boundary fragments and the computation of nodal weights based on physical distance can be erroneous. This issue will become more serious in dealing with the fracture problems, especially for the multiple cracking problems. Several techniques have been reported on the construction of meshfree approximations with discontinuities and non-convex boundaries, including the visibility method [6], the diffraction method [21], and the transparency method [21]. However, these methods are only effective for problems with relatively simple domains (e.g. with one or two cracks, or not many non-convex portions on the boundaries), but not effective for domains with highly irregular boundaries (e.g., with multiple cracks). Liu and Tu [31] have developed a relay model to determine the domain of influence of a node in a complex problem domain.

The relay model is motivated by the way of a radio communication system composed of networks of relay stations. Consider an interpolation domain containing a large number of irregular boundary fragments (or cracks), as shown in Fig. 2, in which O is the interpolation point, P is the field node, and R is the relay point. The field node, e.g., P_2, first radiates its influence in all directions equally, like a radio signal being broadcasted at a radio station, until the contained boundaries are encountered. Then its' influence is relayed through relay points, e.g., R_{2-1} and R_{1-1}, to reach the interpolation point O. The distance (called equivalent distance) between the interpolation point and the field node can then be calculated. The details for the relay model can be found in the book by Liu [3] and paper by Liu and Tu 31].

4. Computation of stress intensity factors

The J integral was introduced by Rice [32], i.e.,

$$J = \int_{\Gamma} \left(w\delta_{1j} - \sigma_{ij} \frac{\partial u_i}{\partial x_1} \right) n_j \, d\Gamma \tag{24}$$

where $w = \frac{1}{2}\sigma_{ij}\varepsilon_{ij}$ is strain energy density. For a mixed mode problem in LEFM, J is related to the stress intensity factors from Irwin's [33] relation,

$$J = \frac{1}{E'}\left(K_I^2 + K_{II}^2\right) \tag{25}$$

where

$$E' = \begin{cases} E, & \text{plane stress} \\ \frac{E}{1-\upsilon^2}, & \text{plane strain} \end{cases} \tag{26}$$

is the effective Young's modulus. K_I and K_{II} donate the stress intensity factors (SIFs) for mode I and mode II, respectively.

The interaction integral was developed to be domain integral based on the J integral which is contour integral, and it is used to extract stress intensity factors [34,35] in LEFM. The procedures are described as follows.

Consider two equilibrium states of a model with crack, status 1 is the actual status for the boundary conditions and status 2 is the auxiliary status.

$$M^{(1,2)} = \int_\Gamma \left[w^{(1,2)}\delta_{1j} - \sigma_{ij}^{(1)}\frac{\partial u_i^{(2)}}{\partial x_1} - \sigma_{ij}^{(2)}\frac{\partial u_i^{(1)}}{\partial x_1} \right] n_j \, \mathrm{d}\Gamma \tag{27}$$

where $M^{(1,2)}$ is the interaction integral, which includes the terms from the actual mixed mode state for the given boundary conditions (superscript 1) and the superimposed near tip auxiliary state (superscript 2).

$$W^{(1,2)} = \frac{1}{2}\left(\sigma_{ij}^{(1)}\varepsilon_{ij}^{(2)} + \sigma_{ij}^{(2)}\varepsilon_{ij}^{(1)}\right) \tag{28}$$

is the mutual strain energy density.

The contour integral can be converted to the domain integral for numerical evaluation.

$$M^{(1,2)} = \int_A \left[\sigma_{ij}^{(1)}\frac{\partial u_i^{(2)}}{\partial x_1} + \sigma_{ij}^{(2)}\frac{\partial u_i^{(1)}}{\partial x_1} - W^{(1,2)}\delta_{1j} \right] \frac{\partial q}{\partial x_j} \, \mathrm{d}A \tag{29}$$

where A is the area of the integral domain, σ_{ij} and u_i are the components of the stress tensor and displacement vector, respectively. $W^{(1,2)}$ is the mutual strain energy from the two states and q is a differentiable function selected to have a value of unity at the crack tip, zero along the boundary of the domain and arbitrary elsewhere.

The function q is selected as follows in this paper

$$q = \left(1 - \frac{2|x|}{c}\right)\left(1 - \frac{2|y|}{c}\right) \tag{30}$$

where c is the length of the square area for interaction integral.

The stress intensity factors can then be evaluated by the interaction integral as

$$K_I = \frac{E'}{2}M^{(1,2)} \tag{31}$$

Note that all quantities are evaluated with respect to the coordinate system with the crack tip as the origin. Following similar process, K_{II} can also be calculated from the above equations.

5. Surface fitting

The performance of a meshfree method firstly depends upon the quality of the meshfree shape functions. Hence the interpolation errors using the enriched RBF meshfree shape function are firstly investigated through surface fitting for given surfaces (functions) [2].

A domain of $(x,y) \in [0,10] \times [0,10]$ is considered for the surface fitting. This domain is represented by 11×11 uniformly distributed field nodes with a constant nodal distance $d_c = 1.0$. A total of 100 points of $(x,y) \in [0.4,9.4] \times [0.4,9.4]$ with distance $h = 1.0$ are considered as interpolation points or sample points; they are intentionally chosen not to coincide with the field nodes to obtain a fair assessment of the fitting accuracy. A rectangular local support domain is used to perform the interpolation for a sample point.

The conventional RBF interpolation with only linear polynomials $\mathbf{p} = \{1\ x\ y\}$ and the enriched RBF interpolation with linear polynomials $\mathbf{p} = \{1\ x\ y\}$ plus 2-terms trigonometric enrichment $\mathbf{T} = \{\sin(\theta)\ \sin(\theta)\cos(\theta)\}^T$ are investigated for the surface fitting. The approximated value of the field function $f(\mathbf{x})$ for each sample point $\mathbf{x}$ can be interpolated using the nodes in the support domain and the meshfree shape functions. The following norms are used as error indicators. The average fitting errors of function values over the entire domain are defined as

$$e_t = \frac{1}{N}\sum_{i=1}^{N}\left|\frac{\tilde{f}_i - f_i}{f_i}\right| \tag{32}$$

where N is the total number of sample points in the entire domain, f_i is the exact values of this function, and $\tilde{f}_i$ is the approximated values of function. In this example, $N = 100$ is used.

The condition number is associated with the linear equation $\mathbf{A} \cdot \mathbf{X} = \mathbf{B}$, it gives a bound on how inaccurate the solution $\mathbf{X}$ will be after approximate solution. It is a parameter to reflect the property/quality of matrix $\mathbf{A}$, which can reveal the method's capacity to construct a good-quality matrix. Larger matrix condition number usually leads to larger approximation error. To compare the difference of condition numbers for the RBF interpolation matrix between conventional and enriched RBFs, the following norm is used

$$e_c = \frac{1}{N}\sum_{i=1}^{N}\left(\frac{E_i - C_i}{C_i}\right) \tag{33}$$

where e_c denotes the difference of condition numbers between the conventional and the enriched RBF interpolations, E_i and C_i are condition numbers of the enriched RBF and the conventional RBF, respectively. $N = 100$ is used in the following study.

5.1. Fitting of a planar surface

A 2-D plane is considered at first, i.e.,

$$f_1(x, y) = x + y + 1.0 \tag{34}$$

It can be observed that both the conventional and the enriched RBF meshfree shape functions can exactly fit the plane to the machine accuracy (10^{-16}). This confirms that the enriched RBF shape functions have remained the linear reproduction property of RBF meshfree shape functions. This linear reproduction property is very important to ensure the convergence of a meshfree method. It should be mentioned here that the planar surface fitting will have errors (10^{-5}–10^{-7}) if the linear polynomial terms are not included in the RBF interpolations. This is because RBF without augmenting the linear polynomial terms cannot exactly reproduce linear polynomials [3]. It has proven the importance of the augment of the linear polynomial in the RBF interpolation.

5.2. Fitting of a complicated trigonometric surface

The following non-polynomial (trigonometric) surface is also fitted using the conventional and the enriched RBF meshfree shape functions.

$$f_2(x, y) = \sin(\theta) + \sin(\theta)\cos(\theta) + 1.5 \tag{35}$$

As illustrated in Table 2, it has found that to fit the above non-polynomial surface, the enriched RBF interpolation augmented with the trigonometric basis functions has very good computational accuracy to 10^{-13}–10^{-16}. For comparison, the conventional RBF shape functions are also used to fit the same surface. As presented in Table 2, the fitting errors resulted from the conventional RBF shape functions are around 10^{-3}, which are much larger than those of the enriched RBF shape functions. It can be concluded that the enriched RBF shape functions can exactly reproduce a trigonometric surface. This property is crucial in the analysis of crack tips because the enriched RBF shape functions can accurately capture the singular stress field of the crack tip, as discussed in Eqs. (1)–(4).

Furthermore, as we can see from Table 2, the condition number differences, e_c, between the enriched RBF interpolation and the conventional RBF interpolation are very small and usually negative. It has proven that, comparing with the conventional RBF interpolation, the enriched RBF interpolation does not lead to increase of the condition number, and even slightly decreases the condition number of the interpolation matrix. Therefore, the enriched RBF interpolation has similar interpolation stability/quality to (or even a little bit better than) the conventional RBF interpolation.

Table 2
Surface fitting results for the trigonometric surface by the enriched RBF meshfree shape functions.

Type of RBFs	$\boldsymbol{e}_t$	Condition numbers	$\boldsymbol{e}_c$ (%)
MQ-RBF			
Conventional	3.50×10^{-3}	10^7–10^{10}	−9.63
Enriched	3.59×10^{-15}		
EXP-RBF			
Conventional	4.10×10^{-3}	10^3–10^5	−5.46
Enriched	1.27×10^{-16}		
TPS-RBF			
Conventional	3.40×10^{-3}	10^7–10^{11}	−8.13
Enriched	3.63×10^{-13}		

Table 3
Comparison of CPU time for conventional and enriched RBF shape functions.

	Enriched RBF (s)	Conventional RBF (s)
Surface fitting	1.007	0.965
Fitting and plotting	2.66	2.55

The computational efficiency of the enriched RBF interpolation is also studied. The CPU time is listed in Table 3. This study is conducted in a HP 6710b Laptop, and the average CPU time of 10 times repeated calculations is taken to reduce the statistical error. As shown in Table 3, it is clearly revealed that the enriched RBF interpolation needs more CPU time than the conventional RBF interpolation, but the difference is small within only around 4%. The increase of the CPU time is resulted from the expansion of the size of the interpolation matrix due to the augmented trigonometric basis functions in the enriched RBF interpolation.

6. e-RPIM for analyses of crack tip fields

In this section, the enriched-RPIM (e-RPIM) is applied to analyze crack tip fields for problems in linear fracture mechanics. The enriched MQ-RBF interpolation with linear polynomials $\mathbf{p} = \{1\ x\ y\}$ plus 4-terms trigonometric enrichment given in Eq. (6) is employed to construct meshfree shape functions. The shape parameters for MQ RBF are $\alpha_c = 1.0$, and $q = 1.03$[2].

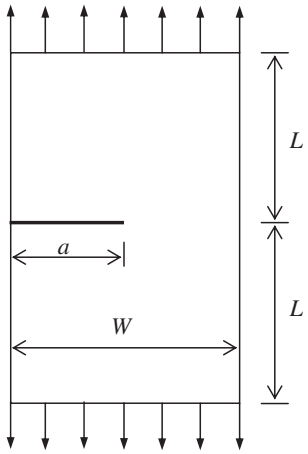

Fig. 3. An edge-cracked rectangular plate subjected to the tension loading.

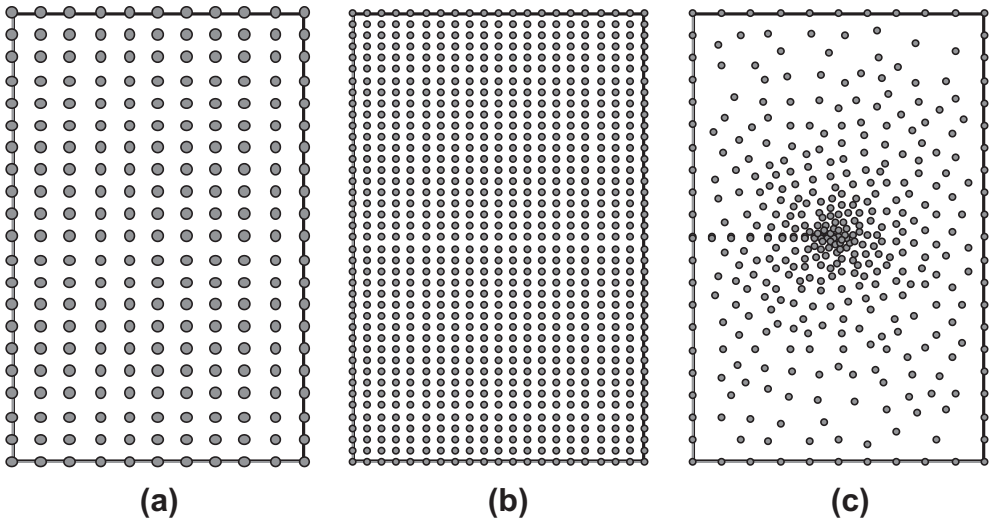

Fig. 4. Nodal distributions: (a) 11 × 21 regular nodes; (b) 21 × 41 regular nodes; (c) 394 irregular nodes generated by the software MFree 2D.

6.1. Mode I single edge-cracked plate

An edge-cracked rectangular plate with the dimension $W = L = 1$ subjected to a uniformed tension of $f = 1.0$, as shown in Fig. 3, is studied. The plane strain condition is considered, and $E = 1000$, $v = 0.25$. The analytical results for K_I had been given by Gdoutos [25] as,

$$K_I = \bar{t}\sqrt{\pi a}\left[1.12 - 0.23\frac{a}{w} + 10.55\left(\frac{a}{w}\right)^2 - 21.72\left(\frac{a}{w}\right)^3 + 30.39\left(\frac{a}{w}\right)^4\right] \tag{36}$$

Table 4
Comparison of the stress intensity factors for mode-I.

a/w	Analytical K_I	e-RPIM (11×21 nodes)		e-RPIM (21×41 nodes)	
		K_I	Error(%)	K_I	Error(%)
0.6	5.53	5.63	1.8	5.60	1.3
0.5	3.54	3.48	−1.7	3.58	1.1
0.4	2.36	2.23	−5.5	2.30	−2.5
0.3	1.61	1.39	−13.7	1.63	1.2
0.2	1.09	0.95	−12.8	1.03	−5.5
0.1	0.66	0.56	−15.2	0.69	4.5

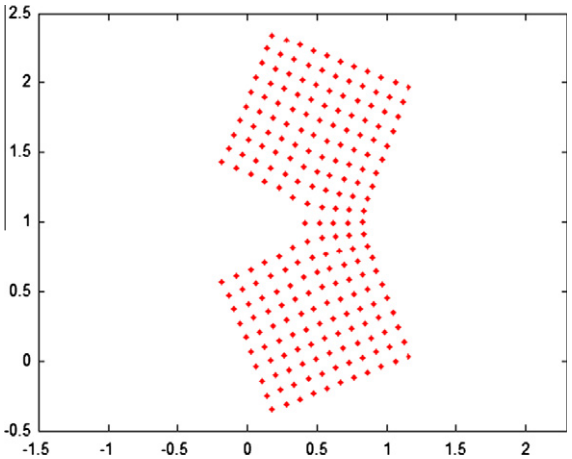

Fig. 5. Schematic deformation enlarged by 50 times (11×21 nodes, $a/W = 0.5$).

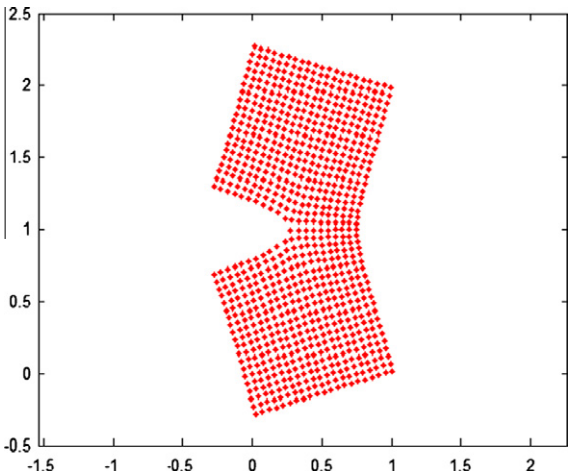

Fig. 6. Schematic deformation enlarged by 50 times (21×41 nodes, $a/W = 0.5$).

The newly developed e-RPIM is employed to simulate this LEFM problem. The problem domain is firstly discretized by regularly distributed 11×21 and 21×41 nodes as shown in Fig. 4a and b. Stress intensity factors are computed using the interaction integral. As listed in Table 4, comparing with the analytical solution in terms of the crack length-width ratio $a/W = 0.1$–0.6, the *e*-RPIM method leads to stable and accurate results as illustrated in Table 4. A schematic deformation is also plotted in Figs. 5 and 6 when $a/W = 0.5$ after 50 times enlargement.

The irregular nodes are also used to simulate this problem. As shown in Fig. 4c, 394 irregular nodes are employed in this study. For $a/w = 0.5$, the irregular nodal distribution leads to $K_I = 3.59$ with error around 1.4%. Therefore, the *e*-RPIM also has good accuracy and stability for the irregular nodes. Robustness for irregular nodal distribution is one of the distinguished advantages of e-RPIM. It should be mentioned here that in Fig. 4c, more field nodes are used surrounding the crack tip. Therefore, this irregular nodal distribution has better effectiveness than the regular nodal distributions, and it can be proven that 394 irregular nodes has led to almost the same computational accuracy as 861 regular nodes (21×41).

6.2. Mode I double edge-cracked plate

A square plate with double edge-cracks, as shown in Fig. 7, is also studied. A total 441 regular nodes are used. Ching and Batra [26] studied the same problem and the analytical K_I given by Gdouos [25] is $(K_I)_{analytical} = 4.65$. Using the interaction integral, the present e-RPIM method leads to $(K_I)_{numerical} = 4.78$, which has a good agreement with the analytical solution.

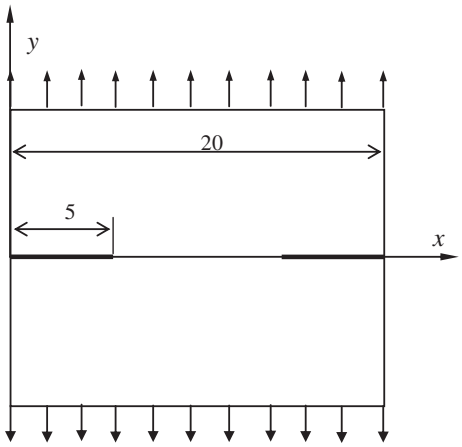

Fig. 7. A double-edge square plate subjected to the tension loading.

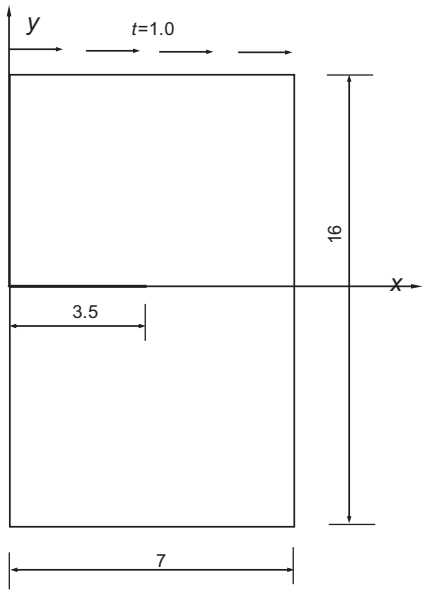

Fig. 8. An edge-cracked plate subjected to the shear loading.

6.2.1. Mode-II edge-cracked plate

An edge-cracked plate is clamped at the bottom and the top end is subjected to a far field shear stress $t = 1.0$, as shown in Fig. 8 with its length $L = 16$ and width $W = 7$. A plane strain state of deformation is assumed. The reference solution for the

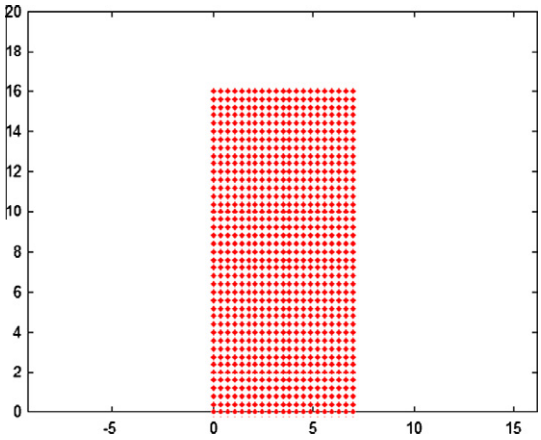

Fig. 9. 21×41 nodal distribution.

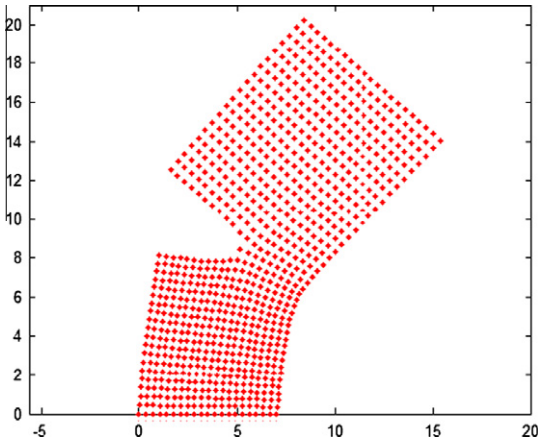

Fig. 10. Schematic deformation enlarged by 10 times (21×41 nodes, $a/W = 0.5$).

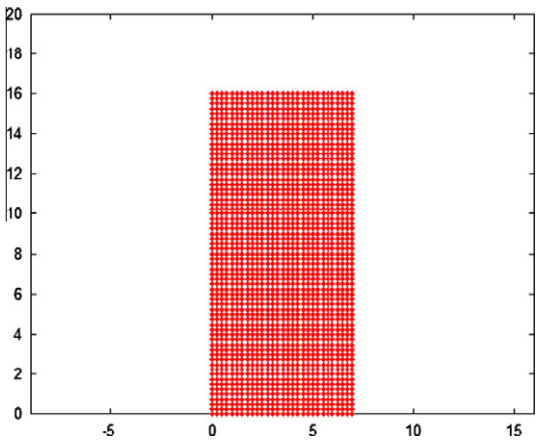

Fig. 11. 29×65 nodal distribution.

stress intensity factors with $a/W = 0.5$ has been given by Fleming et al. [21] and Ching and Batra [26] with $K_I = 34$ and $K_{II} = 4.55$. To obtain the reference solutions for different a/W ratios, FEM with very fine mesh is also employed to simulate the same problem [36]. Two nodal distributions with 21×41 and 29×65 nodes are employed, as shown in Figs. 9 and 11. The predicted stress intensity factors from the proposed e-RPIM method are listed in Table 5. The deformed cracked plate with $a/W = 0.5$ is also plotted schematically in Figs. 10 and 12 after 10 times enlargement. It can be found that a good agreement has been obtained with those from the FEM reference solutions.

6.3. Cracks in a complex shaped plate

As shown in Fig. 13, let us now consider a plate of complex shape with a "C" shaped crack [23]. The material constants used are $E = 3.0 \times 10^7$ and $v = 0.3$. One edge of the plate is fixed, one edge is subjected to uniformly distributed tension load,

Table 5
Comparison of the stress intensity factors for the edge-cracked plate under shear loading on the top.

a/w	FEM		e-RPIM (21×41 nodes)		e-RPIM (29×65 nodes)	
	K_I	K_{II}	K_I	K_{II}	K_I	K_{II}
0.5	34.09	4.54	34.05	4.95	34.12	4.76
0.4	25.8	3.49	22.92	3.08	23.20	3.16
0.3	19.82	2.46	17.13	2.45	19.86	2.52

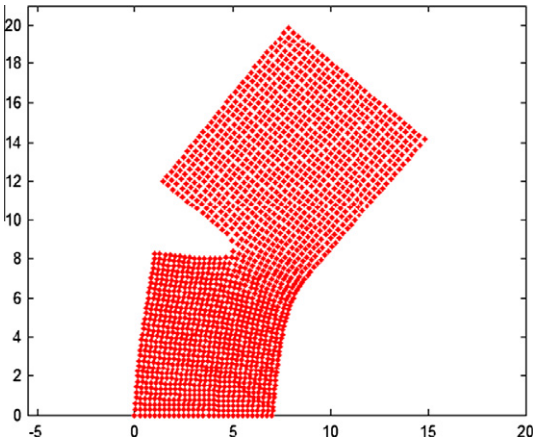

Fig. 12. Schematic deformation enlarged by 10 times (29×65 nodes, $a/W = 0.5$).

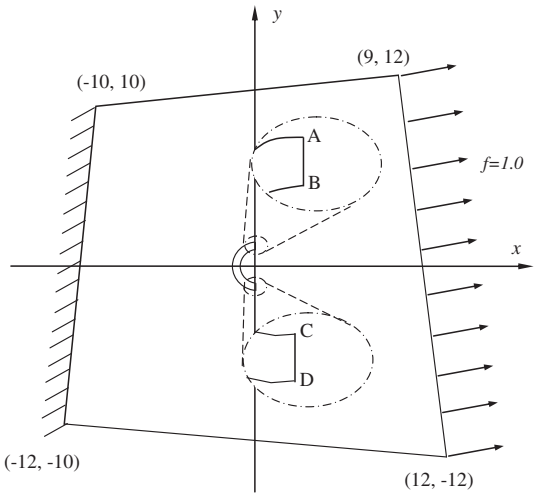

Fig. 13. A plate with a "C" shaped center crack.

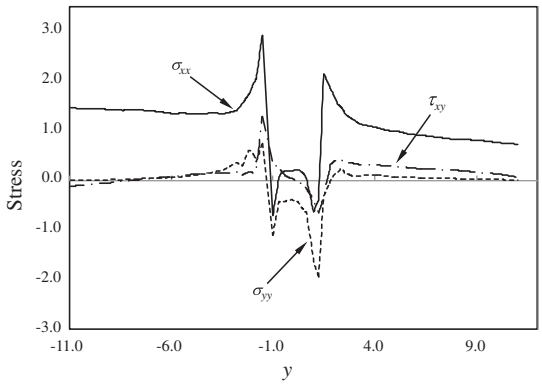

Fig. 14. The stress distributions along the y axis.

and the rests are traction free. The reference solution obtained by the sole meshfree method (the software of MFree 2D: Liu [3]) with very fine nodal distribution has been given by Gu and Zhang [23]. Fig. 14 shows the stress distribution along y-axis, and very good agreement is obtained between the results by the presented e-RPIM and the reference solutions [23]. Actually, if we plot the results in [23] into Fig. 14, curves for σ_{xx} and σ_{yy} obtained in this paper and by Gu et al. are almost identical. The stress concentrations on the crack tips have been clearly shown with the stress concentration factor around 3.4, which was 3.3 reported by Gu and Zhang [23].

7. Conclusion

To handle the stress concentration or singularity is the major challenge in modeling and simulation of fracture problems. Although the meshfree method provides an alternative numerical technique for crack problems, the conventional meshfree method still has difficulty in analysis of crack tips. In this paper, an enriched radial point interpolation method (e-RPIM) is developed for the determination of crack tip fields. The enriched RBF interpolation is proposed through RBF augmenting the suitable trigonometric basis functions in order to reflect the properties of stress fields for the crack tips. Several numerical techniques are developed to ensure the effectiveness for this e-RPIM method. We have drawn the following conclusions:

(a) The surface fitting has proven that comparing with the conventional RBF meshfree shape functions, the enriched RBF meshfree shape functions have: (1) a similar accuracy to fit a polynomial surface; (2) a much better accuracy to fit a trigonometric surface; and (3) a similar interpolation stability due to no increase of the condition number of the interpolation matrix. Therefore, it has proven that the enriched RBF shape functions will not only possess all advantages of the conventional RBF shape functions, but also can accurately reproduce the trigonometric functions.
(b) Several numerical examples have been studied to demonstrate the effectiveness of the present e-RPIM for the analysis of crack tip fields, and very good results have been obtained. The e-RPIM performs better than the conventional RPIM because the relative trigonometric basis functions have been included in construction of enriched RBF shape functions.

Hence, it has been proven that the newly proposed e-RPIM is effective and robust for the analysis of fracture mechanics problems, and it has good potential to become a powerful numerical tool.

References

[1] Liu GR. On G space theory. Int J Comput Methods 2009;6(2):257–89.
[2] Liu GR, Gu YT. An introduction to meshfree methods and their programming. Berlin: Springer Press; 2005.
[3] Liu GR. Mesh free methods: moving beyond the finite element method. 2nd ed. USA: CRC press; 2009.
[4] Zhang X, Liu XH, Song KZ, Lu MW. Least-squares collocation meshless method. Int J Numer Methods Engng 2001;51(9):1089–100.
[5] Gingold RA, Moraghan JJ. Smooth particle hydrodynamics: theory and applications to non spherical stars. Mon Not Roy Astron Soc 1977;181:375–89.
[6] Belytschko T, Lu YY, Gu L. Element-fee Galerkin methods. Int J Numer Methods Engng 1994;37:229–56.
[7] Liu WK, Jun S, Zhang Y. Reproducing kernel particle methods. Int J Numer Methods Engng 1995;20:1081–106.
[8] Liu GR, Gu YT. A point interpolation method for two-dimensional solids. Int J Numer Methods Engng 2001;50(4):937–51.
[9] Atluri SN, Zhu T. A new meshfree local Petrov-Galerkin (MLPG) approach in computational mechanics. Comput Mech 1998;22:117–27.
[10] Liu GR, Gu YT. A local radial point interpolation method (LR-PIM) for free vibration analyses of 2-D solids. J Sound Vib 2001;246(1):29–46.
[11] Mukherjee YX, Mukherjee S. Boundary node method for potential problems. Int J Numer Methods Engng 1997;40:797–815.
[12] Gu YT, Liu GR. A boundary point interpolation method for stress analysis of solids. Comput Mech 2002;28:47–54.
[13] Gu YT, Liu GR. A boundary radial point interpolation method (BRPIM) for 2-D structural analyses. Struct Engng Mech 2003;15(5):535–50.
[14] Liu GR, Zhang GY. Upper bound solution to elasticity problems: a unique property of the linearly conforming point interpolation method (LC-PIM). Int J Numer Methods Engng 2008;74:1128–61.
[15] Liu GR, Gu YT, Dai KY. Assessment and applications of point interpolation methods for computational mechanics. Int J Numer Methods Engng 2004;59(10):1373–97.
[16] Wang JG, Liu GR. A point interpolation meshless method based on radial basis functions. Int J Numer Methods Engng 2002;54:1623–48.

[17] Liu GR. A G space and weakened weak (W2) form for a unified formulation of compatible and incompatible methods, part I – theory and part II – application to solid mechanics problems. Int J Numer Methods Engng 2008.
[18] Liu GR, Dai KY, Nguyen TT. A smoothed finite element method for mechanics problems. Comput Mech 2007;39:859–77.
[19] Liu GR, Nourbakhshnia N, Chen L, Zhang YW. A novel general formulation for singular stress field using the ES-FEM method for the analysis of mixed-mode cracks. Int J Comput Methods 2010;7(1):191–214.
[20] Chen L, Liu GR, Nourbakhsh-Nia N, Zeng K. A singular edge-based smoothed finite element method (ES-FEM) for bimaterial interface cracks. Comput Mech 2010;45(2–3):109–25.
[21] Fleming M, Chu Y, Moran B, Belytschko T. Int J Numer Methods Engng 1997;40:1483–504.
[22] Lu YY, Belytschko T, Tabbara M. Element-free Galerkin method for wave propagation and dynamic fracture. Comput Methods Appl Mech Engng 1995;126:131–53.
[23] Gu YT, Zhang LC. Coupling of the meshfree and finite element methods for determination of the crack tip fields. Engng Fract Mech 2008;75(5):986–1004.
[24] Liu GR, Zhang GY, Gu YT, et al. A meshfree radial point interpolation method (RPIM) for three-dimensional solids. Comput Mech 2005;36(6):421–30.
[25] Gdoutos EE. Fracture mechanics: an introduction. Kluwer Academic Publishers; 1993.
[26] Ching HK, Batra RC. Determination of crack tip fields in linear elastostatics by the meshfree local Petrov-Galerkin (MLPG) method. CMES 2001;2(2):273–89.
[27] Schaback R, Wendland H. Characterization and construction of radial basis functions. In: Dyn N, Leviatan D, Levin D, Pinkus A, editors. Multivariate approximation and applications. Cambridge University Press; 2000.
[28] Gu YT. Meshfree methods and their comparison. Int J Comput Methods 2005;2(4):477–515.
[29] Kansa EJ. Multiquadrics – a scattered data approximation scheme with applications to computational fluid dynamics. Computers Math Applic 1990;19(8/9):127–45.
[30] Liu GR, Gu YT, Dai KY. Assessment and applications of point interpolation methods for computational mechanics. Int J Numer Methods Engng 2004;59(10):1373–97.
[31] Liu GR, Tu ZH. An adaptive procedure based on background cells for meshfree methods. Comput Methods Appl Mech Engng 2002;191:1923–43.
[32] Rice JN. A path independent integral and the approximate analysis of strain concentration by notches and cracks. Comput Meth 1968;35:379–86.
[33] Irwin GR. Analysis of stress and strains near the end of a crack traversing a plate. J Appl Mech 1957;24:361–4.
[34] Yau et al. A mixed-mode crack analysis of isotropic solids using conservation laws of elasticity. J Appl Mech 1980;47:335–41.
[35] Shih, Asaro. Elastic–plastic analysis of cracks on bimaterial interfaces: part I – small scale yielding. J Appl Mech 1988;55:299–316.
[36] Rao BN, Rahman S. Probabilistic fracture mechanics by Galerkin meshless methods – part 1: rates of stress intensity factors. Comput Mech 2002;28:351–64.